Catalysis Today 166 (2011) 91–101

Contents lists available at ScienceDirect

Catalysis Today

journal homepage: www.elsevier.com/locate/cattod

Effect of the support composition on the characteristics of NiMo and CoMo/(Zr)SBA-15 catalysts and their performance in deep hydrodesulfurization

Diego Valencia, Tatiana Klimova*

Facultad de Química, Universidad Nacional Autónoma de México, Cd. Universitaria, Coyoacán, México D.F., 04510, Mexico

ARTICLE INFO

Article history:
Available online 15 September 2010

Keywords:
SBA-15
Zirconia
Mo catalysts
Nickel and cobalt promoters
Deep hydrodesulfurization
Dibenzothiophene
4,6-Dimethyldibenzothiophene

ABSTRACT

In the present work, we tried to get a deeper insight into the effect of the chemical composition of the SBA-15-type support on the development of NiMo and CoMo catalysts in deep hydrodesulfurization (HDS). With this aim, two series of catalysts were prepared using pure silica SBA-15 and ZrO_2-containing SBA-15 as supports. Supports and catalysts were characterized by nitrogen physisorption, small-angle and powder XRD, TPR, UV–vis DRS, HRTEM, and tested in the simultaneous HDS of dibenzothiophene (DBT) and 4,6-dimethyldibenzothiophene (4,6-DMDBT). It was found that the nickel promoter significantly decreased the temperature of reduction of Mo oxide species on both supports used, while the effect of cobalt was relatively small. TPR profiles of Ni/SBA-15 and Co/SBA-15 samples exhibit much smaller metal–support interaction for Co than for Ni. In addition, the presence of agglomerated β-$CoMoO_4$ phase was detected in the XRD pattern of the CoMo/SBA-15 catalyst, whereas the formation of this phase was avoided in the CoMo/ZrSBA-15 sample. TPR results show that zirconia incorporation on the SBA-15 surface significantly increases Co–support interaction and, consequently, the promoter dispersion leading to a better promotion of the MoS_2 active phase. In line with the characterization results, catalytic activity of NiMo catalysts was much higher than those of Mo or CoMo counterparts. In addition, the behavior of Co-promoted Mo/(Zr)SBA-15 catalysts was strongly affected by the chemical composition of the support used, especially in hydrodesulfurization of sterically hindered 4,6-DMDBT. HRTEM study was undertaken to establish how the nature of the promoter as well as the support composition affected the morphology of the active MoS_2 phase and influenced its catalytic behavior.

1. Introduction

Nowadays, the need to improve the removal of sulfur from gasoline and diesel oil by means of deep hydrodesulfurization (HDS) is driven by the new environmental legislation regarding fuel specifications. In many countries, production of ultra-clean diesel fuel with low sulfur content (less than 50 ppm), or even of sulfur-free diesel fuel ($S < 10$ ppm) is currently requested [1]. Attending this demand, many efforts are aimed to design new hydrotreating catalysts, highly active and selective for hydrodesulfurization (HDS) of the refractory polyaromatic sulfur compounds [2–4]. It is known that the active phases of the HDS catalysts are the MoS_2 or WS_2 nanocrystallites promoted by cobalt or nickel atoms, deposited on high specific surface area supports. To modify the efficiency of such complex catalytic systems, different approaches have been tried, for example, the use of novel supports (oxide supports with ordered pore structure, nanostructured materials, etc.) and of novel active phases (noble metals, transition metal phosphides, etc.) or the search for new promoters and additives for the conventional HDS catalysts [5–8]. Among these options, development of novel supports seems to be an interesting and practical option because the support's nature and characteristics play an important role in the catalytic activity. It is well-documented that the support can influence reducibility and sulfidability, structure and dispersion of the deposited metal oxides, as well as the morphology of the sulfided active phases [9].

So far, different mesostructured materials (MCM-41, HMS, FSM-16, KIT-6, etc.) have been tried as supports for HDS catalysts [10–14,5]. Among them, mesoporous molecular sieves of SBA-type, especially the SBA-15 ones [15,16], have attracted much attention in the last few years. These materials have high hydrothermal stability, their textural properties are better than those of the traditional γ-alumina support and the pore size and shape are especially appropriate for the transformation of large organic molecules, such as sulfur-containing compounds of the dibenzothiophene type. At first, pure silica SBA-15 materials were tested as supports for unpromoted Mo(W) catalysts and Co(Ni) promoted ones [17–19]. Obtained results clearly show the advantages of the SBA-15 materials in comparison with the conventionally used γ-alumina support, even though it is well-known that the interaction between silica

* Corresponding author. Tel.: +52 55 56225371; fax: +52 55 56225371.
E-mail address: klimova@servidor.unam.mx (T. Klimova).

0920-5861/$ – see front matter © 2010 Elsevier B.V. All rights reserved.
doi:10.1016/j.cattod.2010.08.006

and Mo(W) species is very weak, and the dispersion of the sulfided active phases is low and inhomogeneous [20]. In further works, attempts to overwhelm the drawbacks of the pure silica SBA-15 support and improve its interaction with HDS active species were made. Thus, it was proposed to modify SBA-15 with different heteroatoms using synthetic or post-synthetic methods [21–30]. In general, improvement of the catalytic activity and some changes in the selectivity were observed when M-SBA-15 supports of different chemical compositions (M = Al, Ti, Zr, W, etc.) were tested. These changes were attributed to an increase in the dispersion of Ni and Mo(W) species and in their reducibility. The most promising results were obtained when Zr- and W-containing SBA-15 materials were used as supports for NiMo and NiW catalysts for deep hydrodesulfurization [23,24,28].

NiMo catalysts supported on zirconia-modified SBA-15 materials showed high performance in HDS of 4,6-dimethyldibenzothiophene (4,6-DMDBT) as well as an increase in the hydrogenation pathway of HDS [22,23]. Murali Dhar and co-workers [24] prepared SBA-15 and ZrO_2-containing SBA-15 materials with zirconia loading between 10 and 50 wt.% and tested them as supports for Mo, CoMo and NiMo catalysts. Catalytic activities of these catalysts were evaluated for hydrodesulfurization of thiophene and hydrogenation (HYD) of cyclohexene. Experimental results revealed different trends in the HDS and HYD activities of the catalysts. For example, HDS of thiophene over Mo, CoMo, and NiMo catalysts increased when SBA-15 was substituted by ZrO_2-SBA-15 with 25 wt.% of zirconia. At the same time, Mo and CoMo/ZrO_2-SBA-15 catalysts showed lower HYD activity than the corresponding catalysts supported on pure silica SBA-15, while the HYD activity of NiMo/ZrO_2-SBA-15 was higher than that of NiMo/SBA-15. A comparison of HDS and HYD activities of CoMo catalysts supported on SBA-15 and TiO_2- and ZrO_2-containing SBA-15 materials also confirmed the above observation, namely, while the incorporation of titania and zirconia into SBA-15 material resulted in an increase in the activity for HDS, activity for HYD decreased. However, when a similar study was made for Mo, CoMo and NiMo catalysts supported on SBA-15 and Al-containing SBA-15 materials with different Si/Al ratios (10–40), it was found that Al-incorporation in the support resulted in an increase in both catalytic activities, in HDS of thiophene and, especially, in HYD of cyclohexene [21]. In one of our recent works, a series of NiMo catalysts supported on SBA-15 materials modified by different metal oxides (MgO, CaO, BaO, Al_2O_3, TiO_2, ZrO_2) were prepared and tested in dibenzothiophene HDS [25]. It was also observed that the support's composition has a strong effect on the catalytic activity and selectivity of the NiMo catalysts.

Resuming the above results, it can be concluded that the catalytic behavior of Mo catalysts in HDS depends in a complex manner not only on the nature of the promoter used, but also on the chemical composition of the SBA-15-type support. In addition, the development of NiMo or CoMo catalysts supported on SBA-15 type materials can also vary in function of a particular S-containing molecule and its own preference towards the possible pathways of HDS. In the present work, we tried to get a deeper insight into the effect of the support's chemical composition on the development of promoted Mo catalysts supported on SBA-15-type materials in deep HDS. With this aim, two series of catalysts were prepared using SBA-15 and ZrSBA-15 as supports. Supports and catalysts were characterized by nitrogen physisorption, small-angle and powder XRD, TPR, UV–vis DRS, HRTEM, and tested in the simultaneous HDS of dibenzothiophene (DBT) and 4,6-dimethyldibenzothiophene (4,6-DMDBT). We selected these two model sulfur-containing compounds because they are representative for the gas oil fraction of petroleum and due to their well-known difference in the preference for a particular pathway of the HDS. Thus, if DBT generally prefers the direct desulfurization pathway (DDS), 4,6-DMDBT is transformed preferentially through the hydrogenation route (HYD).

2. Experimental

2.1. Preparation of supports and catalysts

The pure SBA-15 silica with hexagonal *p6mm* structure was prepared according to literature [15,16] using the triblock copolymer Pluronic P123 (M_{av} = 5800, $EO_{20}PO_{70}EO_{20}$, Aldrich) as the structure-directing agent and tetraethyl orthosilicate (TEOS, Aldrich, 99.999%) as the silica source. Pluronic P123 (4 g) was dissolved in water (30 g) and 2 M HCl (120 g) solution at 35 °C. Then TEOS (8.5 g) was added into the solution. The mixture was stirred at 35 °C for 20 h and then aged at 80 °C for 48 h without stirring. The solid product was recovered by filtration, washed with deionized water and air-dried at room temperature. Calcination was carried out in static air at 550 °C for 6 h. Zirconia-modified SBA-15 support, hereinafter referred to as ZrSBA-15, was prepared by chemical grafting [22]. Zirconium (IV) propoxide (Zr(n-PrO)$_4$, 70 wt.% solution in 1-propanol, Aldrich) was used as the zirconia source and absolute ethanol as the solvent (EtOH, Aldrich, 99.999%). In the grafting procedure, calcined SBA-15 was slurried in EtOH containing Zr(n-PrO)$_4$ for 8 h at room temperature. To eliminate excess of Zr(n-PrO)$_4$, the filtered material was washed with dry EtOH. The solids were dried at room temperature and calcined in static air at 550 °C for 5 h. ZrO_2-content in the synthesized ZrSBA-15 material was found to be 23 wt.% (SEM-EDX).

Mo, NiMo and CoMo catalysts supported on SBA-15 and ZrSBA-15 were prepared by a standard incipient wetness impregnation technique. The calcined supports were impregnated successively using aqueous solutions of ammonium heptamolybdate, $(NH_4)_6Mo_7O_{24}{\cdot}4H_2O$ (Aldrich), and nickel or cobalt nitrates, $Ni(NO_3)_2{\cdot}6H_2O$ or $Co(NO_3)_2{\cdot}6H_2O$ (Aldrich). Mo was impregnated first. After each impregnation, the catalysts were dried first at room temperature (12 h), then at 100 °C (24 h), and, finally, were calcined at 500 °C (4 h). The nominal composition of the catalysts was 12 wt.% of MoO_3 and 3 wt.% of NiO (or CoO). Hereafter, the catalysts will be denoted as Mo, NiMo or CoMo/corresponding support.

2.2. Characterization of supports and catalysts

The supports and catalysts were characterized by N_2 physisorption, X-ray diffraction (XRD), UV–vis diffuse reflectance spectroscopy (DRS), temperature-programmed reduction (TPR), SEM-EDX and HRTEM. N_2 adsorption-desorption isotherms were measured with a Micromeritics ASAP 2000 automatic analyzer at liquid N_2 temperature. Prior to the experiments, the samples were degassed ($p < 10^{-1}$ Pa) at 270 °C for 6 h. Specific surface areas were calculated by the BET method (S_{BET}), the total pore volume (V_p) was determined by nitrogen adsorption at a relative pressure of 0.98 and pore size distributions from the desorption isotherms by the BJH method. The mesopore diameter (D_P) corresponds to the maximum of the pore size distribution. The micropore area (S_μ) was estimated using the correlation of t-Harkins & Jura (*t*-plot method). XRD patterns were recorded in the $3^\circ \leq 2\Theta \leq 90^\circ$ range on a Siemens D5000 diffractometer, using Cu Kα radiation (λ = 1.5406 Å) and a goniometer speed of $1^\circ(2\Theta)\,min^{-1}$. Small-angle XRD ($2\Theta$ = 1–10°) was performed on a Bruker D8 Advance diffractometer using small divergence and scattering slits of 0.05°. The a_0 unit-cell parameter was estimated from the position of the (1 0 0) diffraction line ($a_0 = d_{100} \times 2/\sqrt{3}$) [31]. Pore wall thickness, δ, was assessed by subtracting D_P from the a_0 unit-cell parameter which corresponds to the distance between the centers of adjacent mesopores. UV–vis electronic spectra of the samples were recorded

Table 1
Chemical composition of supports and corresponding Mo, NiMo and CoMo catalysts (wt.%).

Sample	SEM-EDX				Chemical analysis			
	SiO_2	ZrO_2	MoO_3	NiO (CoO)	SiO_2	ZrO_2	MoO_3	NiO (CoO)
SBA-15	100	–	–	–	n.d.[a]	–	–	–
Mo/SBA-15	87.6	–	12.4	–	87.71	–	12.29	–
NiMo/SBA-15	84.8	–	12.2	3.0	84.65	–	12.18	3.17
CoMo/SBA-15	84.9	–	12.0	3.1	84.69	–	12.24	3.07
ZrSBA-15	76.9	23.1	–	–	77.04	22.96	–	–
Mo/ZrSBA-15	67.4	20.3	12.3	–	67.48	20.11	12.41	–
NiMo/ZrSBA-15	65.2	19.7	12.1	3.0	n.d.	n.d.	n.d.	n.d.
CoMo/ZrSBA-15	65.1	19.5	12.2	3.2	65.03	19.54	12.18	3.25

[a] Not determined.

in the wavelength range 200–800 nm using a Varian Cary 100 spectrophotometer equipped with a diffuse reflectance attachment. Polytetrafluoroethylene was used as reference. TPR experiments were carried out in a Micromeritics AutoChem II 2920 automatic analyzer equipped with a TC detector. Before TPR experiments, the samples were pretreated *in situ* at 500 °C for 2 h under air flow and cooled in an Ar stream. The reduction step was performed under a stream of an Ar/H_2 mixture (90/10 mol/mol and 50 ml/min), with a heating rate of 10 °C/min, up to 1000 °C. High resolution transmission electron microscopy (HRTEM) studies were performed using a Jeol 2010 microscope (resolving power 1.9 Å). The solids were ultrasonically dispersed in heptane and the suspension was collected on carbon coated grids. Slab length and layer stacking distributions of MoS_2 crystallites in each sample were established from the measurement of at least 300 crystallites detected on several HRTEM pictures taken from different parts of the same sample dispersed on the microscope grid. Chemical composition of the supports was determined by SEM-EDX using JEOL 5900 LV microscope with OXFORD ISIS equipment. The chemical analysis of the ZrSBA-15 support and selected catalysts was performed by Desert Analytics.

2.3. Catalytic activity

The HDS activity tests were performed in a batch reactor at 300 °C and 7.3 MPa total pressure for 8 h. Prior to the catalytic activity evaluation, the catalysts were sulfided *ex situ* in a tubular reactor at 400 °C for 4 h in a stream of 15 vol.% of H_2S in H_2 under atmospheric pressure. The sulfided catalysts (0.15 g) were transferred in an inert atmosphere (Ar) to a batch reactor (Parr) with 40 mL of hexadecane solution containing the model compounds (DBT, 0.054 mol/L, 2160 ppm of S, and 4,6-DMDBT, 0.012 mol/L, 500 ppm of S). The course of the reaction was followed by withdrawing aliquots each hour and analyzing them on an HP-6890 chromatograph. To corroborate product identification, the product mixture was analyzed on a Hewlett Packard GC–MS instrument.

3. Results and discussion

3.1. Support and catalyst characterization

A zirconia-containing SBA-15 support was prepared from pure silica SBA-15 by chemical grafting technique using a previously described procedure [22]. Zirconia loading in the ZrSBA-15 material determined by SEM-EDX technique and chemical analysis was about 23 wt.% of ZrO_2 which corresponds well to the SBA-15 support covered with a monolayer of highly dispersed zirconia species (Table 1). The textural and structural characteristics of SBA-15 and ZrSBA-15 supports are given in Table 2. The parent SBA-15 material shows surface area of 850 m^2/g, micropore area of 140 m^2/g and total pore volume of 1.13 cm^3/g. Zirconia grafting on the SBA-15 surface results in a decrease of area and pore volume values. Thus, BET surface area decreases to 516 m^2/g and micropore area to 99 m^2/g after Zr(IV) incorporation. Total pore volume and micropore volume follow a similar tendency after Zr(IV) incorporation into SBA-15 support. Such a decrease in the textural characteristics of SBA-15 material can be attributed to an increase in the density of ZrSBA-15 materials with ZrO_2 loading [23]. Fig. 1 shows that Zr(IV) grafting does not produce changes in the characteristic shape of the SBA-15 isotherm (type IV isotherm with an H1 hysteresis loop). Only some decrease in the amount of adsorbed N_2 can be observed indicating that the original pore structure of the parent SBA-15 material is maintained after Zr(IV) incorporation. Small-angle XRD patterns of SBA-15 and ZrSBA-15 samples were found to be similar (Fig. 2). Both supports exhibit three reflections (d_{100}, d_{110} and d_{200}) characteristic for *p6mm* hexagonal symmetry of SBA-15. The position of the SBA-15 reflections and their intensities did not change after Zr(IV) grafting indicating that the

Table 2
Textural and structural characteristics of supports and corresponding Mo, NiMo and CoMo catalysts.

Sample	S_{BET} (m^2/g)	S_{BET} decrease[a] (%)	NS_{BET}[b] (m^2/g)	S_μ[c] (m^2/g)	V_P (cm^3/g)	D_P[d] (Å)	a_0[e] (Å)	δ[f] (Å)
SBA-15	850	–	850	140	1.13	64	110	46
Mo/SBA-15	613	28	700	89	0.83	62	111	49
NiMo/SBA-15	578	32	682	86	0.81	60	112	52
CoMo/SBA-15	602	29	709	68	0.88	62	112	50
ZrSBA-15	516	–	516	99	0.68	56	110	54
Mo/ZrSBA-15	396	23	452	61	0.54	53	110	57
NiMo/ZrSBA-15	366	29	431	46	0.53	53	111	58
CoMo/ZrSBA-15	330	36	390	32	0.51	51	110	59

[a] Decrease in the support surface area (S_{BET}) after deposition of Mo and Ni (Co).
[b] S_{BET} normalized per gram of the corresponding support (SBA-15 or ZrSBA-15).
[c] Micropore area.
[d] Pore diameter determined from the desorption isotherms by the BJH method.
[e] Unit-cell parameter estimated from the position of the (1 0 0) diffraction line ($a_0 = d_{100} \times 2/\sqrt{3}$).
[f] Pore wall thickness ($\delta = a_0 - D_P$).

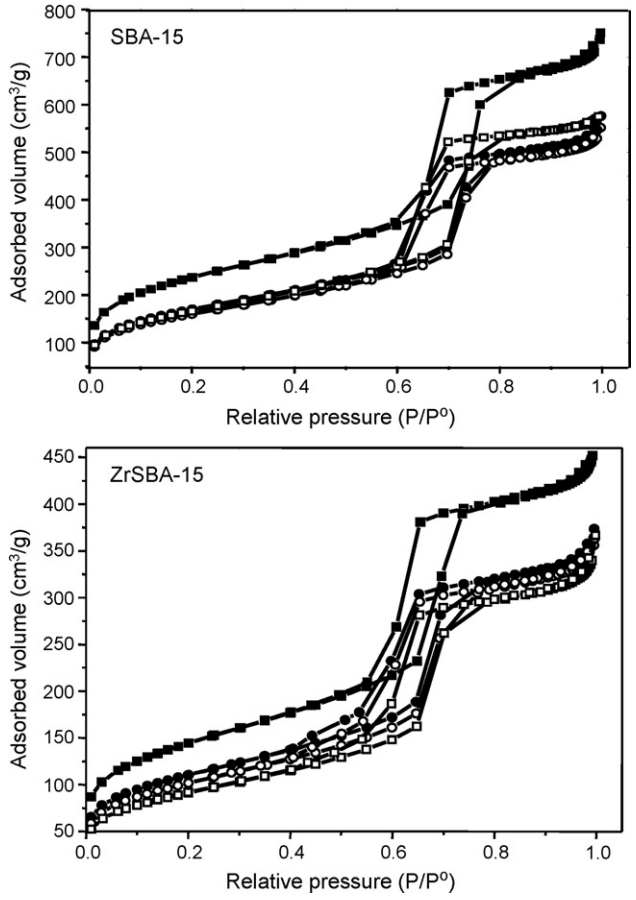

Fig. 1. Nitrogen adsorption–desorption isotherms of (■) SBA-15 or ZrSBA-15 supports and corresponding (●) Mo; (○) NiMo; and (□) CoMo catalysts.

long-range periodicity order of the SBA-15 sample was preserved intact and its unit-cell parameter did not suffer a significant change (Table 2).

The chemical composition and textural characteristics of synthesized Mo, NiMo and CoMo catalysts are given in Tables 1 and 2. Experimentally determined NiO, CoO and MoO_3 loadings in all catalysts were close to the expected ones (Table 1). A significant decrease in BET surface area and total pore volume was observed after Mo and promoter (Ni, Co) incorporation to the supports (Table 2). The form of the N_2 adsorption–desorption isotherm and the shape of the hysteresis loop did not suffer a notable change after successive incorporation of Mo and Ni (Co) species to the SBA-15 and ZrSBA-15 supports (Fig. 1). In line with this, (1 0 0), (1 1 0) and (2 0 0) reflections of *p*6*mm* hexagonal structure of SBA-15 supports were still observed in the small-angle XRD patterns of Mo, NiMo and CoMo catalysts (Fig. 2). The intensity of these reflections becomes lower after Mo and Ni (Co) incorporation (especially for pure silica SBA-15 support), probably because Mo is a strong X-ray absorber [17] or due to some loss of long range order of the support's mesopore structure induced by a partial blocking of the pore channels by the deposited Ni (Co) and Mo oxide species. Results from the calculation of the pore wall thickness for the supports and catalysts (last column, Table 2) confirm that zirconia grafting on the SBA-15 surface, as well as the impregnation of Mo and Ni (Co) oxide species resulted in a small increase in the thickness of the pore walls of the starting SBA-15 support. This indicates that all the metal species mentioned above were deposited mostly inside the SBA-15 mesopore channels.

The X-ray diffraction patterns of the SBA-15 support and corresponding Mo, NiMo and CoMo catalysts in the 2θ interval from 3° to 80° are shown in Fig. 3. The X-ray pattern of the support shows a broad signal between 15° and 35°, which is attributed to the amorphous silica. The XRD pattern of the Mo/SBA-15 catalyst revealed the formation of the crystalline orthorhombic MoO_3 phase (JCPDS card 35-609) pointing out a low dispersion of Mo oxide species on the pure silica support. After the addition of nickel to the Mo/SBA-15 sample, these reflections disappeared indicating an increase in the dispersion of Mo oxide species. However, the addition of cobalt led to a different result. Thus, CoMo/SBA-15 sample exhibited a small peak of β-$CoMoO_4$ phase (JCPDS card 21-868) [32], which overlaps with the broad diffraction of the amorphous support. Similar results have been reported previously for CoMo catalysts supported on different mesoporous silica materials (HMS, MSU and SBA-15) [33–35]. No reflections belonging to molybdenum, nickel or cobalt oxides were observed in the XRD patterns of all catalysts supported on ZrSBA-15 (not shown). This result points out a good dispersion of the deposited metal species in the catalysts supported on ZrSBA-15. A comparison of the XRD results for the

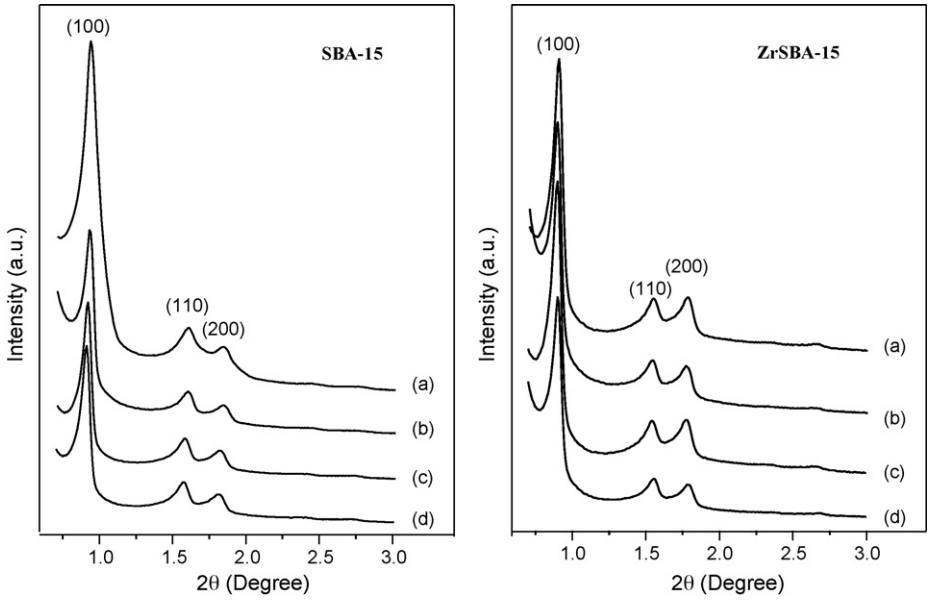

Fig. 2. Small-angle XRD patterns of (a) support; (b) Mo; (c) NiMo; and (d) CoMo catalysts supported on SBA-15 and ZrSBA-15.

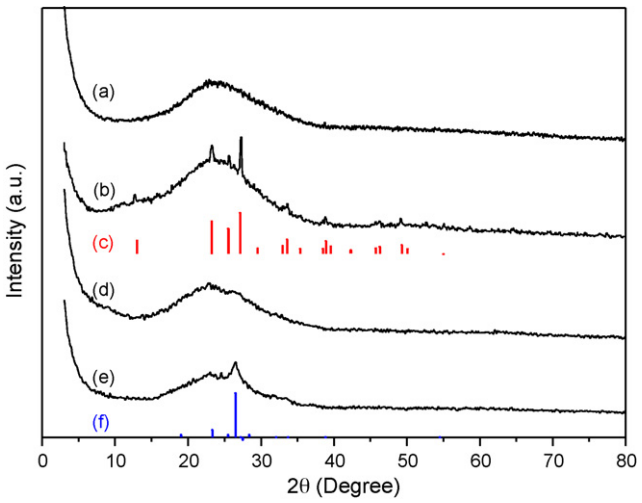

Fig. 3. Powder XRD patterns of (a) SBA-15 support and corresponding (b) Mo/SBA-15, (d) NiMo/SBA-15 and (e) CoMo/SBA-15 catalysts; and reflections of crystalline phases: (c) orthorhombic MoO_3 (JCPDS card 35-609) and (f) β-$CoMoO_4$ (JCPDS card 21-868).

CoMo catalysts supported on SBA-15 and ZrSBA-15 clearly shows that zirconium incorporation into the SBA-15 support resulted in the formation of highly dispersed CoMo phases and inhibited the formation of the crystalline β-$CoMoO_4$ phase.

Further characterization of the catalysts by diffuse reflectance spectroscopy (DRS) and temperature-programmed reduction (TPR) was undertaken in order to inquire more into the characteristics of the deposited Ni, Co and Mo oxide species and their change with the support's composition. UV–vis diffuse reflectance spectra of Mo, NiMo and CoMo catalysts supported on SBA-15 and ZrSBA-15 are shown in Fig. 4. In this figure, absorption bands corresponding to ligand-to-metal charge transfer (LMCT) $O^{2-} \rightarrow Mo^{6+}$ can be observed in the 200–360 nm region. The exact position of these bands reflects the local symmetry around the Mo^{6+} species depending on their coordination and aggregation state [36]. The isolated molybdate species in tetrahedral coordination, Mo(Td), show a characteristic absorption band at ~250 nm, whereas the signal of polymolybdate species in octahedral coordination, Mo(Oh), is observed in the wider region (between 260 and 330 nm) depending on the degree of agglomeration of these species. In addition, both types of Mo^{6+} species show the second strong absorption band at about 220 nm. The spectra of unpromoted Mo/SBA-15 and Mo/ZrSBA-15 catalysts (Fig. 4) clearly demonstrate that the characteristics of Mo oxide species change with the support's composition. Thus, a mixture of Mo oxide species in octahedral and tetrahedral coordination was present in the catalysts supported on pure silica SBA-15. On the ZrSBA-15 support, the Mo catalyst also presents absorption corresponding to both tetrahedral and octahedral Mo^{6+} species. However, the proportion of agglomerated Mo(Oh) species (absorbance between 300 and 330 nm) in this catalyst is significantly lower, whereas the intensity of absorption between 260 and 300 nm is much higher than for the Mo/SBA-15 sample. These changes in the DR spectrum of the Mo catalyst with the incorporation of ZrO_2 in the SBA-15 support can be attributed to an increase in the dispersion of Mo(Oh) species in presence of zirconia. It seems that Ni addition in the Mo/SBA-15 catalyst also produced an increase in the proportion of dispersed octahedral Mo species at the expense of the agglomerated octahedral ones (Fig. 4). So, for the Mo/SBA-15 catalyst, the addition of both Ni promoter and ZrO_2 in the support resulted in an increase in the dispersion of octahedral Mo species. In contrast to the SBA-15-supported Mo and NiMo catalysts, when the ZrSBA-15 material is used as a support, the spectra of Mo and NiMo samples are almost the same (Fig. 4). Therefore, the effect of Ni addition on the dispersion of Mo species is much smaller in this case, probably because a good dispersion of the deposited Mo species has already been achieved in unpromoted Mo/ZrSBA-15 catalyst. Addition of a Co promoter to both Mo catalysts supported on SBA-15 and ZrSBA-15 produced a blue shift of the Mo absorption edge (Fig. 4), which can be due either to an increase in the dispersion of octahedral Mo species in presence of cobalt or to the change in the coordination of the Mo oxide species from octahedral to tetrahedral.

The TPR results for Ni, Mo and NiMo catalysts supported on SBA-15 and ZrSBA-15 are shown in Fig. 5. The reduction profile of the Mo/SBA-15 catalyst shows hydrogen consumption in a broad temperature interval (between 400 and 900 °C) with three main reduction peaks at 531, 632 and 762 °C. The low-temperature peak (531 °C) can be attributed to the first step of reduction (from Mo^{6+} to Mo^{4+}) of polymeric octahedral Mo species weakly bound to the silica surface (probably small clusters of MoO_3) [37,38]. In addition, hydrogen consumption at an intermediate temperature (632 °C) can be ascribed to the reduction of octahedral Mo^{6+} species of the crystalline MoO_3 phase detected by XRD [38]. The peak at about 762 °C can be ascribed to the second step of reduction of the octahedral Mo species of different degrees of agglomeration (from Mo^{4+} to Mo^0) and to the first step of reduction of isolated tetrahedral Mo^{6+} species in strong interaction with the support [37,38]. The above reduction profile of the Mo/SBA-15 catalyst is well in line with previous results obtained for similar Mo catalysts supported on other ordered mesoporous silicas (for example, Mo/MCM-41 [39]) and with its DRS characterization, where the presence of different types of oxide Mo species was detected. When Ni was added in the Mo/SBA-15 catalyst, three principal changes were observed in the reduction behavior of the Mo oxide species: a considerable decrease in the temperature corresponding to the main reduction peak (from 531 °C for Mo/SBA-15 to 404 °C for NiMo/SBA-15), disappearance of the second reduction peak observed at 632 °C for the Mo/SBA-15 sample and a strong increase in the hydrogen consumption at a low-temperature region (320–500 °C). All the above indicates an increase in the proportion of easy to reduce dispersed octahedral Mo species at the expense of tetrahedral ones. For the Mo and NiMo catalysts supported on ZrSBA-15 (Fig. 5), the reduction of Mo^{6+} species occurs at lower temperature in comparison with that on the pure silica support. Thus, for the unpromoted Mo catalyst, one main peak at 477 °C with a shoulder at 635 °C were observed and attributed to the first and second steps of reduction of dispersed octahedral Mo^{6+} species. Nickel addition to the Mo/ZrSBA-15 catalyst leads to further decrease in the temperatures of reduction of octahedral Mo oxide species (from 477 °C for the Mo/ZrSBA-15 to 365 °C for the corresponding Ni-promoted sample). Among all catalysts studied, the NiMo/ZrSBA-15 catalyst showed the presence of Mo oxide species reducible at the lowest temperature. The above results indicate that the effect of the Ni promoter is similar in the case of the pure silica SBA-15 and zirconia-containing SBA-15 supports. It appears that in both cases the reason for this is the better dispersion of Mo species in presence of nickel. Another interesting observation can be made from the results shown in Fig. 5, when the TPR profiles of the Ni samples supported on SBA-15 and ZrSBA-15 are compared. The Ni/SBA-15 sample exhibits one broad low-temperature reduction region (200–500 °C) that can be ascribed to the reduction ($Ni^{2+} \rightarrow Ni^0$) of octahedrally coordinated Ni^{2+} species weakly bound to the silica surface [39]. When zirconia is added to the SBA-15 support, Ni oxide species are reduced at a significantly higher temperature (between 300 and 600 °C) and a new reduction peak with a maximum at about 514 °C appears in the TPR profile of the Ni/ZrSBA-15 sample as a result of the stronger interaction of nickel species with the zirconia-containing support. Therefore, zirconia addition to the SBA-15 support leads, on the

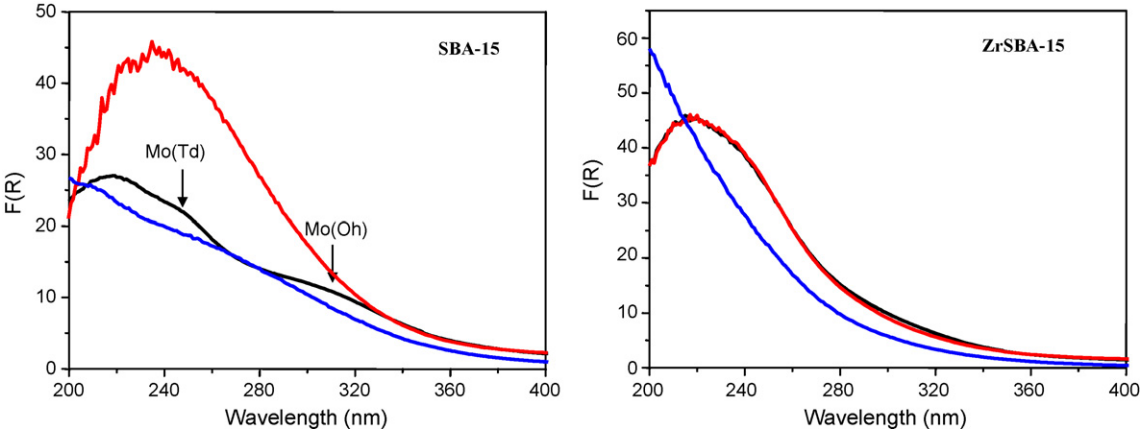

Fig. 4. UV–vis diffuse reflectance spectra of Mo (black line), NiMo (red line) and CoMo (blue line) catalysts supported on SBA-15 and ZrSBA-15. (For interpretation of the references to color in this figure legend, the reader is referred to the web version of the article.)

one hand, to an increase in the temperature of reduction of the Ni^{2+} species, and on the other, to a decrease in the temperature of reduction of the Mo oxide species. As a result, the reduction of both Ni and Mo oxide species on the ZrSBA-15 support takes place almost in the same temperature interval (between 300 and 700 °C) which probably could favor the formation of a mixed NiMoS phase during the activation of the NiMo/ZrSBA-15 catalyst.

The TPR results for Co, Mo and CoMo catalysts supported on SBA-15 and ZrSBA-15 shown in Fig. 6 indicate that the effect that the addition of the cobalt promoter has on the ease of reduction of Mo oxide species is much smaller than that of nickel. Only a decrease of about 10–50 °C in the temperature of reduction of octahedral Mo species is observed for ZrSBA-15 and pure silica SBA-15 supports, respectively. So it can be assumed that the effect that the cobalt promoter has on the dispersion of octahedral Mo oxide species was not as strong as that of nickel. However, some other differences were detected in the reduction behavior of the CoMo catalysts supported on SBA-15 and on the Zr-containing support, namely a notable increase in hydrogen consumption near 600 °C in the TPR profile of the CoMo/ZrSBA-15 sample. According to literature [38], reduction of crystalline MoO_3 phase takes place at this temperature; however, in the case of our CoMo/ZrSBA-15 catalyst, the formation of this crystalline phase was not detected by powder XRD. DRS characterization also pointed out a good dispersion of Mo species in this sample. Probably this reduction peak can be attributed to the reduction of mixed CoMo oxide species formed on this Zr-containing support; however, this supposition needs further experimental confirmation. The Co/SBA-15 catalyst has one well-defined reduction peak at 295 °C with a shoulder at about 480 °C, which could be assigned to the stepwise reduction of Co_3O_4 ($Co^{3+} \rightarrow Co^{2+} \rightarrow Co^0$) [40–42]. When zirconia is added to the SBA-15 support, Co reduction takes place at a substantially higher temperature (515 and 690 °C, Fig. 6). This shift in the reduction temperature of Co oxide species can be ascribed to an interaction between cobalt and zirconia, which replaces the cobalt-silica interaction [43,44]. In addition, a comparison of the TPR profiles of Co/SBA-15 (main reduction peak at 295 °C) and Ni/SBA-15 (main reduction peak at about 400 °C) renders evident that the interaction of cobalt with the pure silica SBA-15 is much smaller than that of nickel. Probably, this very small interaction of Co species with the SBA-15 support is a reason for the formation of the β-$CoMoO_4$ phase detected by powder XRD in the CoMo/SBA-15 catalyst. When the SBA-15 support was modified by ZrO_2 incorporation, a significant increase in the temperature of Ni^{2+} and Co^{2+} reduction was observed. However, this increase was much stronger for the cobalt (around 200–220 °C) than for the nickel promoter (~100 °C). In line with this, formation of the β-$CoMoO_4$ phase was avoided on the zirconia-containing support. Resuming all above results, it can be concluded that the change in the chemical composition of the SBA-15 support due to the incorporation of zirconia affects much more strongly the Co–support interaction than the Ni-support one and this could also have implications in the molybdenum promotion by Ni or Co species and its catalytic behavior.

HRTEM characterization of sulfided Mo, NiMo and CoMo catalysts was performed in order to get more information about the dispersion of catalytically active MoS_2 species. Fig. 7 shows the HRTEM micrographs of unpromoted and Ni- or Co-promoted Mo catalysts supported on SBA-15 and ZrSBA-15. Fig. 8 shows

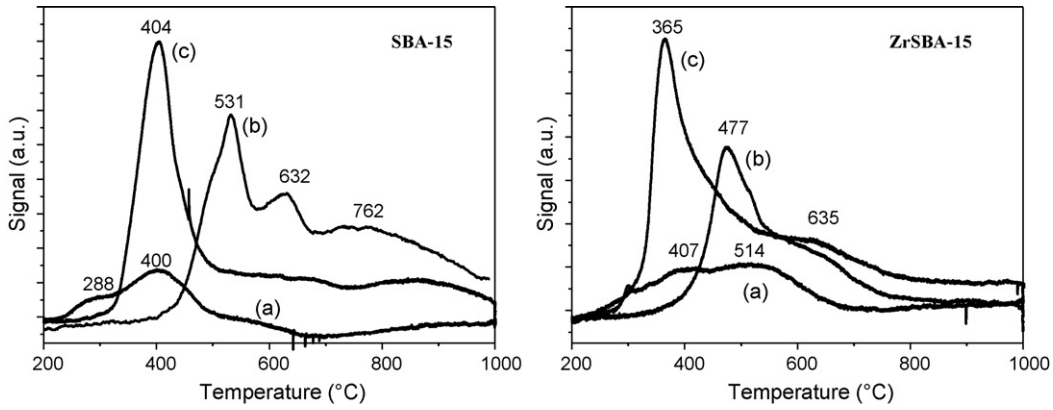

Fig. 5. TPR profiles of (a) Ni, (b) Mo and (c) NiMo catalysts supported on SBA-15 and ZrSBA-15.

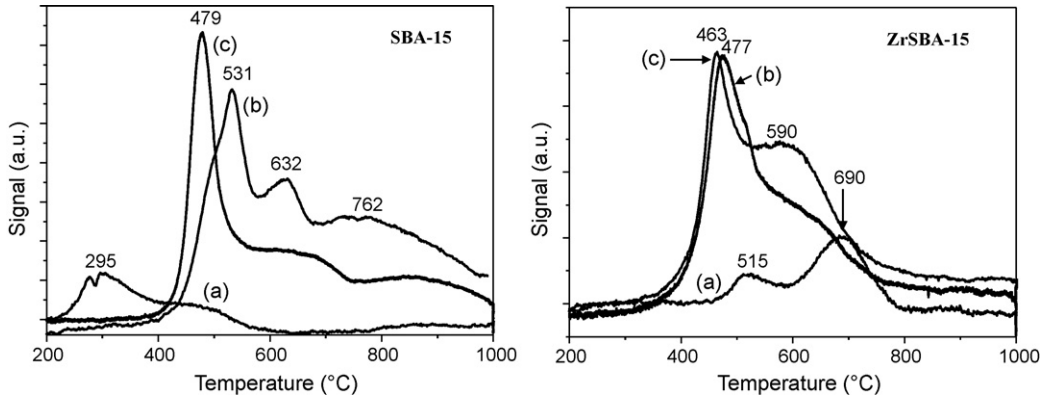

Fig. 6. TPR profiles of (a) Co, (b) Mo and (c) CoMo catalysts supported on SBA-15 and ZrSBA-15.

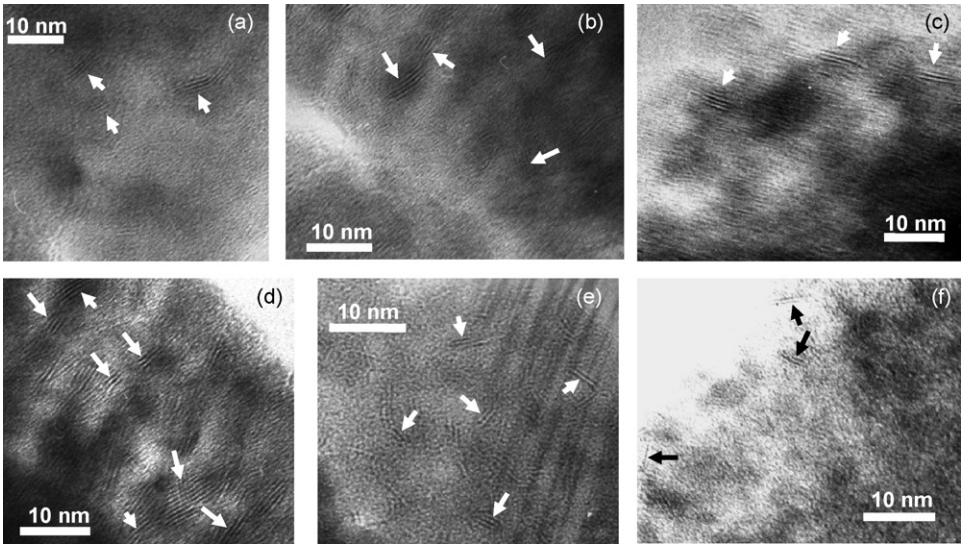

Fig. 7. HRTEM micrographs of sulfided catalysts: (a) Mo/SBA-15, (b) NiMo/SBA-15, (c) CoMo/SBA-15, (d) Mo/ZrSBA-15, (e) NiMo/ZrSBA-15, and (f) CoMo/ZrSBA-15.

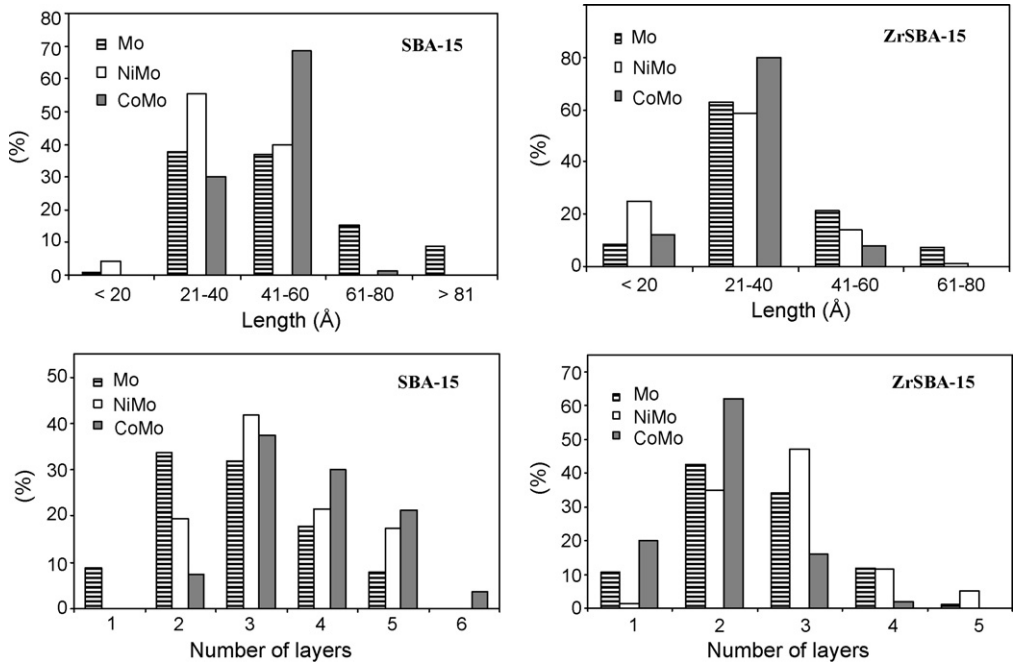

Fig. 8. Length and layer stacking distributions of MoS_2 crystallites in sulfided Mo, NiMo and CoMo catalysts supported on SBA-15 and ZrSBA-15.

the slab length and stacking degree distributions for the same catalysts. The typical fringes due to MoS_2 crystallites with 6.1 Å interplanar distances were observed on micrographs of all sulfided catalysts. Inhomogeneous dispersion of the MoS_2 phase can be seen in the unpromoted Mo catalyst supported on siliceous SBA-15 (micrograph (a), Fig. 7). In this case, MoS_2 crystallites with lengths between 20 and 80 Å and stacking from one to five layers were observed (Fig. 8). In addition, some very large MoS_2 crystals (500–2000 Å) were also found on the external surface of SBA-15 particles (not shown). Nickel addition to this catalyst resulted in better dispersion and more homogeneous distribution of MoS_2 crystals (Figs. 7(b) and 8). Particles with lengths between 20 and 60 Å and stacking from 2 to 5 layers are predominant in this case. When cobalt was used instead of nickel, larger MoS_2 particles were observed with length between 40 and 60 Å and stacking from 3 to 5 layers (Fig. 7(c)). Zirconium incorporation in the support resulted, as expected, in better dispersion of MoS_2 active phase (Fig. 7(d)–(f)). It can be clearly observed that in general in ZrSBA-15-supported catalysts the dispersion of the MoS_2 active phase is much better and more homogeneous than in the catalysts with similar metal loading supported on pure silica SBA-15 (Fig. 8). Zirconia addition in the support produced a decrease in the average stacking degree and length of MoS_2 particles (Table 2). Short MoS_2 particles (30–36 Å) were formed predominantly in the sulfided Mo, NiMo and CoMo/ZrSBA-15 catalysts. However, some differences in the stacking degree can be observed between these three catalysts. It seems that the sulfided NiMo/ZrSBA-15 catalyst is formed by more stacked particles of the active phase than the corresponding unpromoted and Co-promoted Mo/ZrSBA-15 analogs (Table 3).

3.2. Catalytic activity in deep HDS

In the present study, catalytic activity of Mo, NiMo and CoMo catalysts supported on SBA-15 and ZrSBA-15 was tested in simultaneous hydrodesulfurization of dibenzothiophene (DBT) and 4,6-dimethyldibenzothiophene (4,6-DMDBT). These two sulfur-containing molecules were selected as characteristic examples of the refractory sulfur compounds contained in the gas oil fraction of petroleum [45]. It is known that the HDS of DBT-type derivatives occurs through two parallel reactions (Fig. 9), namely, (i) direct desulfurization (DDS) yielding the corresponding products of biphenyl-type, and (ii) hydrogenation with subsequent desulfurization (HYD), yielding first pre-hydrogenated intermediates (tetrahydrodibenzothiophenes, and then the corresponding hexahydro-derivatives) and, finally, cyclohexylbenzene-type compounds [46,47]. It has been shown that under HDS conditions (*i.e.*, in presence of an organic sulfur compound) biphenyl-type products do not hydrogenate readily into cyclohexylbenzene-type ones [48].

The conversions of DBT and 4,6-DMDBT obtained over Mo, NiMo and CoMo catalysts supported on SBA-15 are shown in Fig. 10. It can be observed that DBT conversion reached at 8 h changes in a wide range. The lowest conversion (30.3%) was obtained with the unpromoted Mo/SBA-15 catalyst. Catalytic activities of both Ni- and Co-promoted Mo catalysts supported on SBA-15 resulted to be significantly higher than that of the Mo/SBA-15 catalyst (Table 4). Thus, 68% of DBT conversion was obtained at 8 h reaction time with the NiMo/SBA-15 catalyst and 43.8% with the CoMo one. However, these DBT conversions were still lower than that obtained with the reference NiMo/γ-Al_2O_3 sample. The conversion of 4,6-DMDBT was also increased after the addition of nickel to the Mo/SBA-15 catalyst. In contrast, the behavior of the CoMo/SBA-15 in HDS of 4,6-DMDBT was quite different. Surprisingly, the Co-promoted catalyst had a slightly lower activity for the elimination of this sterically hindered molecule than the unpromoted Mo/SBA-15 sample. These activity trends should be related with the characteristics of the Ni- and Co-promoted Mo/SBA-15 catalysts described above. Thus, the low activity of the Co-promoted sample is due probably to the formation of the agglomerated β-$CoMoO_4$ phase detected by XRD. On the other hand, in the Ni-promoted Mo/SBA-15 sample, Mo oxide and sulfided species were found to be better dispersed than in the corresponding unpromoted Mo catalyst (Table 3), which explains its higher activity in the DBT and 4,6-DMDBT hydrodesulfurization.

Fig. 11 and Table 4 show the catalytic activity of Mo, NiMo and CoMo catalysts supported on ZrSBA-15 in DBT and 4,6-DMDBT hydrodesulfurization. It can be clearly observed that ZrO_2 loading in the SBA-15 support resulted in an increase in the activity of all three catalysts in HDS of the sulfur-containing model compounds used. DBT conversions higher than 90% were reached at 8 h reaction time over both NiMo and CoMo/ZrSBA-15 catalysts, whereas the conversion of 4,6-DMDBT was higher than 80% over the Ni-promoted catalyst and more than 70% over the corresponding Co-promoted sample. The NiMo/ZrSBA-15 catalyst resulted to be the most active among all the catalysts tested, including the reference NiMo/γ-Al_2O_3 sample, for the HDS of both DBT and 4,6-DMDBT. This result seems to be in accordance with the TPR characterization of this catalyst. Although the Co-promoted Mo catalysts were less active than the Ni-promoted counterparts, the effect of zirconia addition to the SBA-15 support was more beneficial for the CoMo catalyst than for the NiMo one. This can be clearly noted comparing the difference in the activity of the CoMo catalysts supported on the SBA-15 and the ZrSBA-15 (Table 4). For both model compounds used (DBT and 4,6-DMDBT), the CoMo catalyst's activity increased more than twice after the addition of ZrO_2 to the SBA-15 support. The difference in the activity of the NiMo catalysts supported on SBA-15 and ZrSBA-15 was smaller (about 50–60%). The magnitude of the above changes in the activity of the NiMo and CoMo catalysts after ZrO_2 incorporation in the SBA-15 supports seems to be related to the strength of the promoter–zirconia interaction which was larger for Co than for Ni (as it was shown by TPR).

To elucidate the effect of Ni and Co promoters on the selectivity of the Mo catalysts supported on SBA-15 and ZrSBA-15 in HDS of DBT and 4,6-DMDBT, the reaction product distributions were compared for different catalysts (Tables 5 and 6). The product distributions obtained for the unpromoted Mo catalysts supported on both SBA-15 and ZrSBA-15 show a high proportion of pre-hydrogenated intermediates in the products of DBT (Table 5) and 4,6-DMDBT (Table 6) transformations, especially for the Mo/ZrSBA-15 sample. This is in accordance with the results of our previous study [23], in which it was also observed that zirconium(IV) incorporation into the SBA-15 support resulted in an increase in the hydrogenation ability of the Mo catalysts, in addition to an increase in their overall activity. However, unpromoted Mo catalysts, even supported on Zr-containing SBA-15 materials, were not able to realize efficiently the C–S bond cleavage leading to sulfur elimination especially from the pre-hydrogenated intermediates of 4,6-DMDBT. Addition of the promoters (Ni and Co) to the Mo catalysts supported on SBA-15 and ZrSBA-15 resulted in a significant increase in hydrogenolysis reactions leading to an increase in the proportion of the sulfur-free products. The ratios of the prin-

Table 3
Average length and average stacking degree of MoS_2 crystallites in different catalysts.

Catalyst	Average length (Å)	Average stacking (number of layers)
Mo/SBA-15	48	2.8
NiMo/SBA-15	38	3.4
CoMo/SBA-15	43	3.8
Mo/ZrSBA-15	36	2.5
NiMo/ZrSBA-15	31	2.8
CoMo/ZrSBA-15	30	2.0

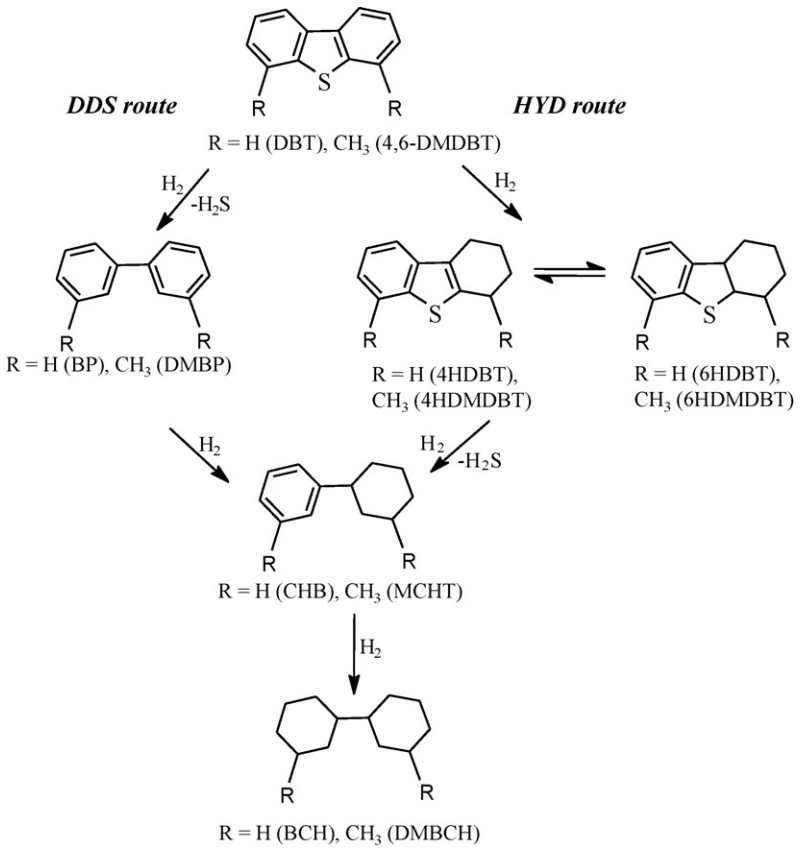

Fig. 9. General reaction network for hydrodesulfurization of dibenzothiophenes. DBT, dibenzothiophene; 4,6-DMDBT, 4,6-dimethyldibenzothiophene; 4HDBT, tetrahydrodibenzothiophene; 4HDMDBT, tetrahydrodimethyldibenzothiophene; 6HDBT, hexahydrodibenzothiophene; 6HDMDBT, hexahydrodimethyldibenzothiophene; BP, biphenyl; DMBP, dimethylbiphenyl; CHB, cyclohexylbenzene; MCHT, methylcyclohexyltoluene; BCH, bicyclohexyl; DMBCH, dimethylbicyclohexyl.

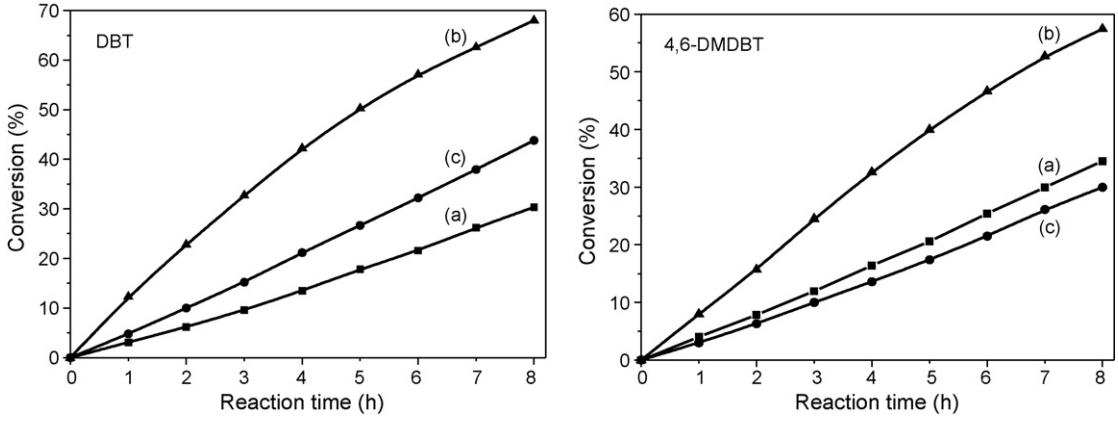

Fig. 10. DBT and 4,6-DMDBT conversions obtained over (a) Mo, (b) NiMo and (c) CoMo catalysts supported on SBA-15.

Table 4
Activity of Mo, NiMo and CoMo catalysts supported on SBA-15 and ZrSBA-15 in hydrodesulfurization of DBT and 4,6-DMDBT at 300 °C.

Catalyst	Pseudo-first-order rate constant (L/(s × $g_{cat.}$))		DBT conversion (%)		4,6-DMDBT conversion (%)	
	DBT	4,6-DMDBT	4 h[a]	8 h	4 h	8 h
Mo/SBA-15	2.5×10^{-6}	3.0×10^{-6}	13.5	30.3	16.4	34.5
NiMo/SBA-15	7.8×10^{-6}	6.0×10^{-6}	42.2	68.0	32.6	57.5
CoMo/SBA-15	3.9×10^{-6}	2.5×10^{-6}	21.2	43.8	13.6	30.0
Mo/ZrSBA-15	3.6×10^{-6}	4.3×10^{-6}	19.4	35.3	23.0	47.8
NiMo/ZrSBA-15	12.7×10^{-6}	9.7×10^{-6}	68.5	94.5	52.3	86.4
CoMo/ZrSBA-15	10.3×10^{-6}	6.8×10^{-6}	55.5	91.5	36.7	72.7
NiMo/γ-Al_2O_3	12.6×10^{-6}	5.2×10^{-6}	68.1	92.0	28.0	55.1

[a] Reaction time.

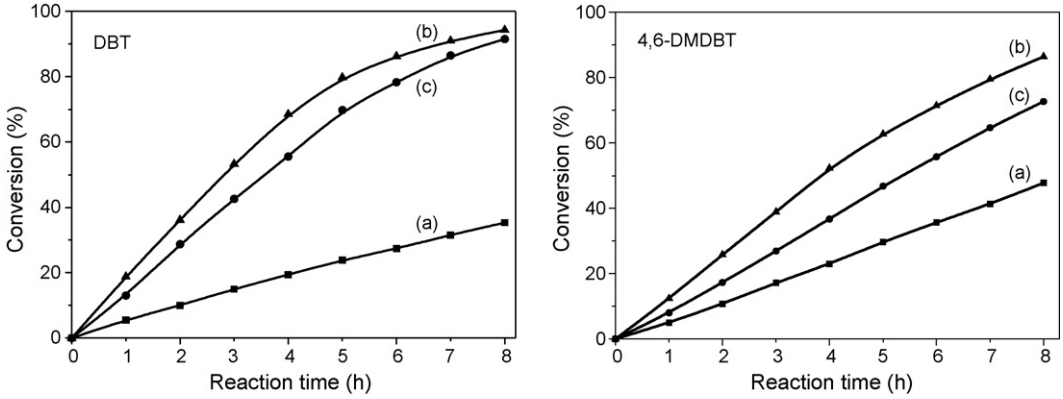

Fig. 11. DBT and 4,6-DMDBT conversions obtained over (a) Mo, (b) NiMo and (c) CoMo catalysts supported on ZrSBA-15.

Table 5
Selectivity of Mo, NiMo and CoMo catalysts in hydrodesulfurization of dibenzothiophene (at 30% of DBT conversion).

Catalyst	t_{30}[a] (h)	Products[b] (%)				Reaction product ratios		
		4HDBT	BP	CHB	BCH	BP/4HDBT[c]	CHB/4HDBT[d]	BP/(CHB + BCH)[e]
Mo/SBA-15	8.0	9	41	49	1	4.6	5.4	0.8
NiMo/SBA-15	2.7	7	47	44	2	6.7	6.3	1.0
CoMo/SBA-15	5.8	4	70	26	0	17.5	6.5	2.7
Mo/ZrSBA-15	6.7	20	36	44	0	1.8	2.2	0.8
NiMo/ZrSBA-15	1.5	7	50	42	1	7.1	6.0	1.2
CoMo/ZrSBA-15	2.2	2	75	23	0	37.5	11.5	3.3
NiMo/γ-Al_2O_3	1.7	7	66	27	0	9.4	3.8	2.4

[a] Time required to reach 30% of DBT conversion.
[b] 4HDBT, tetrahydrodibenzothiophene; BP, biphenyl; CHB, cyclohexylbenzene; BCH, bicyclohexyl.
[c] BP/4HDBT ratio represents the ratio of the catalyst's abilities for hydrogenolysis and for hydrogenation of DBT.
[d] CHB/4HDBT ratio characterizes the catalyst's ability for sulfur elimination from the pre-hydrogenated 4HDBT intermediate.
[e] BP/(CHB + BCH) represents the ratio of the desulfurized product obtained via the DDS pathway to those obtained via the HYD pathway.

cipal desulfurized products (BP/(CHB + BCH)) from Table 5 show that for all Ni- or Co-promoted catalysts studied, the preferential pathway of DBT hydrodesulfurization is the direct desulfurization. Cobalt promoter especially favors this route. The maximum BP/4HDBT and BP/(CHB + BCH) ratios (37.5 and 3.3 respectively) were reached with the CoMo catalyst supported on the ZrSBA-15, probably because of the formation of a larger amount of the Co-promoted Mo species in this catalyst due to an appropriate Co–support interaction. Regarding the product distributions obtained for the hydrodesulfurization of 4,6-DMDBT (Table 6), the preferential pathway of HDS, as expected, was found to be the HYD route. Methylcyclohexyltoluene (MCHT) was the principal desulfurized product obtained with all the catalysts tested. Addition of nickel and, especially, of cobalt promoters also enhanced the cleavage of the C–S bond in the pre-hydrogenated products of 4,6-dimethyldibenzothiophene. The lowest proportion of the tetrahydro- and hexahydro-dimethyldibenzothiophenes was obtained with the CoMo catalyst supported on the ZrSBA-15. It seems that the low hydrogenation ability of the Co-promoted Mo catalysts limits their overall activity in the HDS of refractory sulfur-containing compounds, such as 4,6-DMDBT, which because of steric hindrance prefers the HYD pathway of the reaction.

The described above activity and selectivity trends observed in the simultaneous HDS of DBT and 4,6-DMDBT molecules over Ni or Co-promoted Mo catalysts supported on SBA-15 and ZrSBA-15 materials seem to be related to the dispersion of oxide and sulfided molybdenum phases, as well as to the proportion of the Ni (Co)-promoted MoS_2 species. The dispersion of Mo species increases with the addition of the Ni promoter to both Mo/SBA-15 and Mo/ZrSBA-15 samples, while the effect of the cobalt promoter is enhanced when the ZrO_2-containing SBA-15 support is used, probably due to a stronger Co–zirconia interaction. In addition, the

Table 6
Selectivity of Mo, NiMo and CoMo catalysts in 4,6-DMDBT hydrodesulfurization (at 30% of 4,6-DMDBT conversion).

Catalyst	t_{30}[a] (h)	Products[b] (%)					Product ratios	
		4H	6H	DMBP	MCHT	DMBCH	MCHT/(4H + 6H)[c]	DMBP/(MCHT + DMBCH)[d]
Mo/SBA-15	7.0	44	13	8	29	6	0.5	0.23
NiMo/SBA-15	3.8	27	8	9	46	10	1.3	0.16
CoMo/SBA-15	8.0	8	4	15	65	8	5.4	0.20
Mo/ZrSBA-15	5.0	54	15	7	21	3	0.3	0.29
NiMo/ZrSBA-15	2.4	27	0	7	53	13	2.0	0.11
CoMo/ZrSBA-15	3.4	7	0	17	67	9	9.6	0.22
NiMo/γ-Al_2O_3	4.4	17	0	15	55	13	3.2	0.22

[a] Time required to reach 30% of 4,6-DMDBT conversion.
[b] 4H, tetrahydrodimethyldibenzothiophene (4HDMDBT); 6H, hexahydrodimethyldibenzothiophene (6HDMDBT); DMBP, dimethylbiphenyl; MCHT, methylcyclohexyltoluene; DMBCH, dimethylbicyclohexyl.
[c] MCHT/(4H + 6H) ratio characterizes the catalyst ability for sulfur elimination from the pre-hydrogenated intermediates.
[d] DMBP/(MCHT + DMBCH) represents the ratio of the desulfurized product obtained via the DDS pathway to those obtained via the HYD pathway.

temperature of reduction of the dispersed octahedrally coordinated Mo^{6+} species in the NiMo/ZrSBA-15 catalyst was the lowest among all the catalysts tested. Therefore, the highest total amount of HDS active sites can be expected in this catalyst in comparison with all other tested samples, which explains its highest HDS activity.

4. Conclusions

In the present work, Ni- and Co-promoted Mo catalysts supported on SBA-15 and ZrSBA-15 mesoporous ordered materials were characterized and tested in the simultaneous HDS of dibenzothiophene and 4,6-dimethyldibenzothiophene. It was found that the chemical composition of the SBA-15 support used has a very strong effect on the behavior of the promoted Mo catalysts in deep hydrodesulfurization, especially of sterically hindered molecules such as 4,6-DMDBT.

The Ni promoter significantly decreased the temperature of reduction of oxide Mo species on both supports used, while the effect of Co addition on Mo^{6+} reduction was relatively small. In line with the characterization results, catalytic activity of Ni-promoted Mo catalysts was much higher than that of unpromoted or Co-promoted counterparts.

The presence of the agglomerated β-$CoMoO_4$ phase was detected by powder XRD in the CoMo/SBA-15 catalyst. However, the formation of this phase was avoided when the SBA-15 support was modified by ZrO_2, due to an increase in the Co interaction with the ZrO_2-containing support.

Acknowledgements

Financial support by CONACYT-Mexico (grant 100945) is gratefully acknowledged. The authors thank M. Aguilar Franco, C. Salcedo Luna and I. Puente Lee for technical assistance with small-angle XRD, powder XRD and electron microscopy characterizations, respectively.

References

[1] Y. Yoshimura, M. Toba, H. Farag, K. Sakanishi, Catal. Surv. Asia 8 (2004) 47.
[2] C. Song, Catal. Today 86 (2003) 211.
[3] L. Vradman, M.V. Landau, M. Herskowitz, Catal. Today 48 (1999) 41.
[4] K.G. Knudsen, B.H. Cooper, H. Topsøe, Appl. Catal. A: Gen. 189 (1999) 205.
[5] K. Soni, B.S. Rana, A.K. Sinha, A. Bhaumik, M. Nandi, M. Kumar, G.M. Dhar, Appl. Catal. B: Environ. 90 (2009) 55.
[6] J.A. Toledo-Antonio, M.A. Cortés-Jácome, C. Angeles-Chávez, J. Escobar, M.C. Barrera, E. López-Salinas, Appl. Catal. B: Environ. 90 (2009) 213.
[7] T.I. Korányi, A.E. Coumans, E.J.M. Hensen, R. Ryoo, H.S. Kim, É. Pfeifer, Z. Kasztovszky, Appl. Catal. A: Gen. 365 (2009) 48.
[8] E. Kraleva, A. Spojakina, K. Jiratova, L. Petrov, Catal. Lett. 112 (2006) 203.
[9] Y. Okamoto, M. Breysse, G.M. Dhar, C. Song, Catal. Today 86 (2003) 1.
[10] F. Zhou, X. Li, A.J. Wang, L.Y. Wang, X.D. Yang, Y.K. Hu, Catal. Today 150 (2010) 218.
[11] A. Montesinos-Castellanos, T.A. Zepeda, Micropor. Mesopor. Mater. 113 (2008) 146.
[12] T.A. Zepeda, T. Halachev, B. Pawelec, R. Nava, T. Klimova, G.A. Fuentes, J.L.G. Fierro, Catal. Commun. 7 (2006) 33.
[13] S. Garg, T. Bhaskar, K. Soni, G.M. Kumaran, A. Muto, Y. Sakatab, G.M. Dhar, Chem. Commun. 42 (2008) 5310.
[14] K. Soni, K.C. Mouli, A.K. Dalay, J. Adjaye, Catal. Lett. 136 (2010) 116.
[15] D. Zhao, J. Feng, Q. Huo, N. Melosh, G.H. Fredrickson, B.F. Chmelka, G.D. Stucky, Science 279 (1998) 548.
[16] D. Zhao, Q. Huo, J. Feng, B.F. Chmelka, G.D. Stucky, J. Am. Chem. Soc. 120 (1998) 6024.
[17] A. Sampieri, S. Pronier, J. Blanchard, M. Breysse, S. Brunet, K. Fajerwerg, C. Louis, G. Pérot, Catal. Today 107–108 (2005) 537.
[18] G. Murali Dhar, G. Muthu Kumaran, M. Kumar, K.S. Rawat, L.D. Sharma, B. David Raju, K.S. Rama Rao, Catal. Today 99 (2005) 309.
[19] L. Vradman, M.V. Landau, M. Herskowitz, V. Ezersky, M. Talianker, S. Nikitenko, Y. Koltypin, A. Gedanken, J. Catal. 213 (2003) 163.
[20] E.J.M. Hensen, P.J. Kooyman, Y. van der Meer, A.M. van der Kraan, V.H.J. de Beer, J.A.R. van Veen, R.A. van Santen, J. Catal. 199 (2001) 224.
[21] G. Muthu Kumaran, S. Garg, K. Soni, M. Kumar, L.D. Sharma, G. Murali Dhar, K.S. Rama Rao, Appl. Catal. A: Gen. 305 (2006) 123.
[22] O.Y. Gutiérrez, G.A. Fuentes, C. Salcedo, T. Klimova, Catal. Today 116 (2006) 485.
[23] O.Y. Gutiérrez, D. Valencia, G.A. Fuentes, T. Klimova, J. Catal. 249 (2007) 140.
[24] S. Garg, K. Soni, G. Muthu Kumaran, M. Kumar, J.K. Gupta, L.D. Sharma, G. Murali Dhar, Catal. Today 130 (2008) 302.
[25] T. Klimova, L. Peña, L. Lizama, O.Y. Gutiérrez, C. Salcedo, Ind. Eng. Chem. Res. 48 (2009) 1126.
[26] T. Klimova, J. Reyes, O. Gutiérrez, L. Lizama, Appl. Catal. A: Gen. 335 (2008) 159.
[27] O.Y. Gutiérrez, F. Pérez, G.A. Fuentes, X. Bokhimi, T. Klimova, Catal. Today 130 (2008) 292.
[28] R. Palcheva, A. Spojakina, L. Dimitrov, K. Jiratova, Micropor. Mesopor. Mater. 122 (2009) 128.
[29] A. Olivas, T.A. Zepeda, Catal. Today 143 (2009) 120.
[30] T. Klimova, O. Gutiérrez, L. Lizama, J. Amezcua, Micropor. Mesopor. Mater. 133 (2010) 91.
[31] T. Yamada, H. Zhou, K. Asai, I. Honma, Mater. Lett. 56 (2002) 93.
[32] D. Cauzzi, M. Deltratti, G. Predieri, A. Tiripicchio, A. Kaddouri, C. Mazzocchia, E. Tempesti, A. Armigliato, C. Vignali, Appl. Catal. A: Gen. 182 (1999) 125.
[33] T.A. Zepeda, J.L.G. Fierro, B. Pawelec, R. Nava, T. Klimova, G.A. Fuentes, T. Halachev, Chem. Mater. 17 (2005) 4062.
[34] A. Infantes-Molina, J. Mérida-Robles, E. Rodríguez-Castellón, J.L.G. Fierro, A. Jiménez-López, J. Catal. 240 (2006) 258.
[35] R. Nava, B. Pawelec, J. Morales, R.A. Ortega, J.L.G. Fierro, Micropor. Mesopor. Mater. 118 (2009) 189.
[36] R.S. Weber, J. Catal. 151 (1995) 470.
[37] R. López Cordero, A. López Agudo, Appl. Catal. A: Gen. 202 (2000) 23.
[38] R. López Cordero, F.J. Gil Llambias, A. López Agudo, Appl. Catal. 74 (1991) 125.
[39] T. Klimova, M. Calderón, J. Ramírez, Appl. Catal. A: Gen. 240 (2003) 29.
[40] P. Arnoldy, J.A. Moulijn, J. Catal. 93 (1985) 38.
[41] D. Yin, W. Li, W. Yang, H. Xiang, Y. Sun, B. Zhong, S. Peng, Micropor. Mesopor. Mater. 47 (2001) 15.
[42] A.M. Venezia, R. Murania, G. Pantaleo, G. Deganello, J. Mol. Catal. A: Chem. 271 (2007) 238.
[43] A. Feller, M. Claeys, E. van Steen, J. Catal. 185 (1999) 120.
[44] A. Infantes-Molina, J. Mérida-Robles, E. Rodríguez-Castellón, B. Pawelec, J.L.G. Fierro, A. Jiménez-López, Appl. Catal. A: Gen. 286 (2005) 239.
[45] B.C. Gates, H. Topsøe, Polyhedron 16 (1997) 3213.
[46] C. Pophal, F. Kameda, K. Hoshino, S. Yoshinaka, K. Segawa, Catal. Today 39 (1997) 21.
[47] F. Bataille, J.L. Lemberton, P. Michaud, G. Pérot, M. Vrinat, M. Lemaire, E. Schulz, M. Breysse, S. Kasztelan, J. Catal. 191 (2000) 409.
[48] P. Michaud, J.L. Lemberton, G. Pérot, Appl. Catal. A: Gen. 169 (1998) 343.